Journal of Fluid Mechanics

http://journals.cambridge.org/FLM

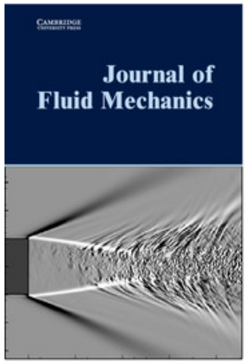

Bottom pressure distribution due to wave scattering near a submerged obstacle

Julien Touboul and Vincent Rey

Journal of Fluid Mechanics / Volume 702 / July 2012, pp 444 - 459
DOI: 10.1017/jfm.2012.193, Published online: 07 June 2012

J. Fluid Mech. (2012), *vol.* 702, *pp.* 444–459.
doi:10.1017/jfm.2012.193

Bottom pressure distribution due to wave scattering near a submerged obstacle

Julien Touboul† and Vincent Rey

Mediterranean Institute of Oceanography (MIO), Aix-Marseille Univ, Université du Sud Toulon-Var, CNRS/INSU, MIO UMR 7294, IRD, MIO UMR235, 83957, La Garde CEDEX, France

(Received 30 September 2011; revised 4 April 2012; accepted 16 April 2012; first published online 7 June 2012)

The dynamic pressure distribution on the bottom of a wave flume, due to the interaction of water waves with a submerged structure, is investigated experimentally and analytically, for both first- and second-order gravity waves of finite amplitude. The dynamic pressure excess is found to be very important, even for incoming waves propagating in deep water conditions. In this depth condition, a high pressure zone, thirty times larger than the dynamic pressure excess expected in the absence of the obstacle, is found in its vicinity. On the other hand, a low pressure zone is observed in the vicinity of the submerged obstacle for incoming waves propagating in smaller depth conditions. In any case, pressure gradients remain important. The second-order disturbance is found to be larger than first order in deep water conditions, for some specific conditions and locations. This result is interpreted in terms of nonlinear coupling of first-order components, including local modes.

Key words: coastal engineering

1. Introduction

Although surface water waves have been widely studied during the last two hundred years, they still raise interesting questions, from both physical and mathematical points of view. This fact is especially well illustrated when considering the interaction between waves and the seabed. Among other issues, the evaluation of the bottom dynamic pressure excess due to surface waves is of major interest. Knowledge of this pressure term, regardless of the hydrostatic pressure, has several motivations.

Among the applications, one may cite the prediction of seabed stability, which is of central importance in coastal engineering (Silvester & Hsu 1989). Common approaches aiming to predict seabed stability focus on the determination of the Keulegan–Carpenter number (Sumer, Whitehouse & Torum 2001). This non-dimensional number involves the fluid velocity at the bottom, and is independent of the pressure forcing applied at the water–sediment interface. However, ever since the work of Yamamoto *et al.* (1978) it has been known that the sediment should not be treated as a rigid bed ruled by Darcy's law. The oscillating pressure term on top of the sediment layer, which corresponds to the boundary condition applied above the poro-elastic media, has to be known. To estimate this pressure forcing, several authors have suggested models based on the linear theory of water waves. One may cite

† Email address for correspondence: julien.touboul@univ-tln.fr

Tsai (1995) and Lee & Lan (2002), who considered counter-propagative modes in the vicinity of a submerged breakwater. These authors suggested a stability criterion based on that assumption. More recently, Lan *et al.* (2011) studied the interaction of surface water waves with poro-elastic breakwaters, taking into account the linear propagative components of water waves. All these studies neglected local modes, and second-order nonlinear effects.

Another application for knowledge of the wave-induced pressure excess is the measurement of surface water waves based on pressure data recorded under water. The use of these transducers is of great interest, since they are less prone to damage by human activities (Grace 1978). Several authors have discussed the ability of linear theory to describe surface waves, since the pressure induced by surface waves decreases with the depth of submersion of the transducer (Cavaleri 1980). Several techniques overcoming this difficulty have been suggested (Wang, Lee & Garcia 1986; Nielsen 1989). However, at the same time, Bishop & Donelan (1987) conducted a very well-documented experiment demonstrating the ability of linear theory to reconstruct surface elevation in shallow water and intermediate depth. More recently, Tsai *et al.* (2005) have introduced a depth parameter correcting the linear transfer function. Escher & Schlurmann (2008) obtained this depth parameter rigorously, assuming the presence of propagative linear modes. Here again, none of these studies considered the influence of local modes, which might be present once the transducer is located in the vicinity of abrupt bathymetries or coastal structures.

Furthermore, the literature cited above only addresses waves propagating in shallow water or in intermediate depths. This makes sense, since the pressure oscillations associated with propagative modes, in linear theory, decrease exponentially with depth. But surprisingly, water waves have long been suspected of inducing bottom pressure disturbances in deep water (Wiechert 1904). The induced seismic noise, called microseisms, is known to oscillate at twice the frequency of the waves. This phenomenon remained unexplained until the experimental demonstration of this correlation (Miche 1944). A realistic theory of this coupling was introduced by Longuet-Higgins (1950), and extended to random waves by Hasselmann (1963). The theory rests on the second-order nonlinear interaction of counter-propagative modes on the surface, which results in a pressure term independent of depth. The first detailed verification of this theory was performed by Kedar *et al.* (2008). Recently, Ardhuin *et al.* (2011) introduced a model of seismic noise, based on the deterministic simulation of water wave propagation. These authors distinguished three cases capable of generating counter-propagative wave systems. They included the reflection of water waves due to the presence of the coast. Several authors have tried to take advantage of this property. We may cite Farrell & Munk (2008, 2010), who analysed the wind wave spectrum from deep sea pressure records, or Molin *et al.* (2008), who suggested that wave energy might be tapped using the Longuet-Higgins effect. Here again, none of these studies took the role of local modes into account, since the only propagative modes are assumed to be present at the sea surface.

In coastal areas, however, local or evanescent modes are known to play a significant role in the dynamics of water waves. This role was made evident through laboratory experiments for water waves interacting with a doubly sinusoidal bed, particularly near the subharmonic Bragg resonance (Guazzelli, Rey & Belzons 1992). For field study applications, the role of local modes on water waves propagating over rapidly changing bathymetries was discussed by Magne *et al.* (2007) through the analysis of wave propagation over the Scripps Canyon. Field experiments were compared to theoretical models such as the coupled-mode models (Athanassoulis & Belibassakis

1999) and the stepwise model (Rey 1992), both of which include the influence of evanescent modes. In the work of Magne *et al.* (2007), the comparison between the experiments and the analytical model showed non-trivial behaviour for water waves, and emphasized the role of local modes on the dynamics.

Regarding the bottom pressure excess, local modes might also be expected to play an important role. Similarly to the Longuet-Higgins term, the velocity potential associated with local modes does not vanish with depth. Although these modes are widely used to analyse the forces exerted by waves on structures (Grue & Palm 1984; Belibassakis & Athanassoulis 2006), the dynamic pressure excess they induce at the bottom has never been analysed. Similarly, the effect of the horizontal oscillation of water under a solid boundary (Guevel *et al.* 1986) has a velocity potential expression that does not vanish with depth. It might also have an important effect on the dynamic pressure distribution on the bottom, even in deep water conditions.

The purpose of this work is to describe the bottom pressure distribution in the vicinity of a submerged obstacle interacting with incident monochromatic waves, and to emphasize the role of local modes at first and second order in nonlinearity. The experimental set-up is presented in § 2. In § 3, we present the model used to analyse the results. This model is based on analytical solutions of the linear problem in domains of constant depth. In its classical formulation, the model is forced by an incident wave of fundamental frequency f. This formulation is useful to describe the dynamic pressure distributions related to this frequency. However, following the results of Miche (1944) and Longuet-Higgins (1950), it is plausible that the second-order terms (related to the second harmonic of frequency $2f$) might make an important contribution, and should be described. We thus suggest an extension of the model to second order in nonlinearity. The interaction of incident and reflected waves, corresponding to the term initially introduced by Longuet-Higgins (1950), is taken into account here, together with the interaction of propagative and local modes. This approach extends classical analytical integral formulations (e.g. Newman 1990), which neglect the influence of local modes, and which are often used to describe the far-field second-order harmonics radiated from a body, or wave forces exerted on a body. Finally, experimental results obtained are compared with results predicted by the model, and discussed in § 4.

2. Experimental set-up

The Ocean Engineering Basin (BGO) FIRST is designed to conduct ocean and coastal engineering model studies. Its useful length is 24 m, while its effective width is 16 m. The bottom of the basin is mobile, allowing the bathymetry to be adapted. It can be inclined up to ±7 % for coastal engineering studies with variable bottom topography. The maximum water depth is 5 m, although a 10 m depth pit, of diameter 5 m, can be used to study structures in deep water. Water waves can be generated by means of a surface wavemaker, covering the entire width of the basin. The wavemaker is composed of horizontally oscillating cylinders, allowing production of regular and irregular waves in the presence of currents. The wave frequency extends from 0.3 to 1.4 Hz, while the maximum crest-to-trough wave height is 0.8 m. At the other end of the basin, a parabolic permeable wave absorber of extend 7 m dissipates wave energy. A carriage can be moved over the useful length of the entire basin. It allows the quick installation and repositioning of the instrumentation.

The coordinate system is Cartesian. The (Ox) axis is parallel to the wave propagation direction, along the basin, the origin being the upstream edge of the

$N°$	1	2	3	4	5	6	7	8	9
T (s)	1.4	1.4	1.4	1.9	1.9	1.9	2.7	2.7	2.7
a_i (mm)	44	54	65	60	99	117	37	71	98
kh	6.16	6.16	6.16	3.35	3.35	3.35	1.76	1.76	1.76
ε	0.09	0.11	0.13	0.07	0.11	0.13	0.02	0.04	0.06

TABLE 1. List of experiments conducted.

Sensor	W_1	W_2	W_3	W_4	W_5	W_6	W_7	W_8	W_9
x (m)	2.985	3.785	4.285	6.085	6.685	6.985	7.150	7.450	7.750
z (m)	0	0	0	0	0	0	0	0	0
Sensor	W_{10}	W_{11}	W_{12}	W_{13}	W_{14}	W_{15}	W_{16}	W_{17}	W_{18}
x (m)	8.050	8.350	8.515	9.115	9.715	10.315	10.915	11.415	12.215
z (m)	0	0	0	0	0	0	0	0	0
Sensor	P_3	P_4	P_5	P_6	P_7	P_8	P_9	P_{10}	P_{11}
x (m)	4.285	6.085	6.685	6.985	7.150	7.450	7.750	8.050	8.350
z (m)	−3	−3	−3	−3	−3	−3	−3	−3	−3
Sensor	P_{12}	P_{13}	P_{14}	P_{15}	P_{16}	P_{17}	P_{18}		
x (m)	8.515	9.115	9.715	10.315	10.915	11.415	12.215		
z (m)	−3	−3	−3	−3	−3	−3	−3		

TABLE 2. Location of the wave probes $(W_n)_{n=1,\ldots,18}$ and the pressure sensors $(P_n)_{n=3,\ldots,18}$.

mobile bottom. The (Oy) axis is parallel to the basin width, its origin being the axis of symmetry of the basin. The (Oz) axis is vertical, oriented upwards. Its origin is the still water level.

In the framework of this study, the mobile bottom was raised to maintain a constant water depth of $h_1 = 3$ m. The structure considered consists of a 1.53 m long plate, 0.1 m thick. The plate is located between $X_6 = 6.985$ m (corresponding to wave probe W_6) and $X_{12} = 8.515$ m (corresponding to wave probe W_{12}). Its topside immersion depth is 0.5 m. To avoid three-dimensional effects, the plate extends over the complete width of the basin. This structure was used in this configuration in a former work (Rey & Touboul 2011), for the study of the hydrodynamical interaction with gravity waves. Waves considered in the present experiment are monochromatic. Their periods are $T_1 = 1.4$ s, $T_2 = 1.9$ s and $T_3 = 2.7$ s, and three wave amplitudes are considered for each case. The waves of period T_1 correspond to waves propagating in deep water conditions, while the waves of period T_2 and T_3 propagate in finite water. A list of the experiments conducted is detailed in table 1. In the table, a_i refers to the amplitude of the incident water wave, while $\varepsilon = a_i k$ is the corresponding wave steepness, given for reference.

The synchronous instrumentation is composed of 18 wave probes $(W_n)_{n=1,\ldots,18}$ and 16 pressure sensors $(P_n)_{n=3,\ldots,18}$. The locations of the sensors are detailed in table 2, while a sketch of the experimental set-up is given in figure 1. The wave probes are resistive sensors, manufactured by HR Wallingford. They deliver a ± 10 V signal, allowing a precision of 10^{-3} m in determining the water elevation. The pressure sensors are piezo-resistive sensors, manufactured by STS. The full scale of measurement ranges from 0 to 400 mbar. Resolution of the pressure sensors is 0.2 mbar.

The evaluation of incident wave amplitude a_i, and of reflected wave amplitude a_r is based on the method initially introduced by Goda & Suzuki (1976) and later

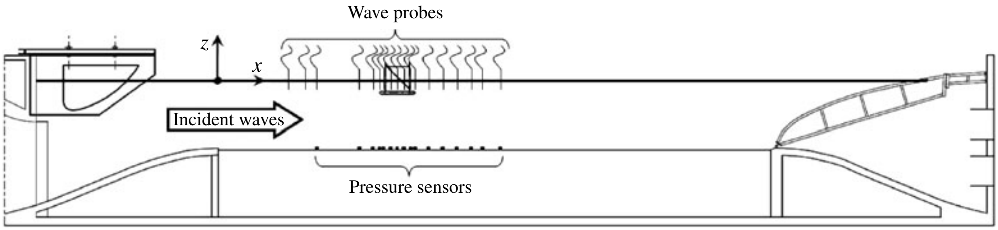

FIGURE 1. Side view of the experimental set-up.

improved by Mansard & Funke (1980). The method is based on the variation of surface elevation envelope, interpreted as the interaction of counter-propagating waves between three probes. A limitation of the method due to spacing of wave probes is studied in Rey, Capiobianco & Dulou (2002). The spacing of probes W_1, W_2 and W_3 was chosen to overcome this drawback.

3. Analytical model

The stepwise model was initially introduced by Takano (1960) to describe water waves propagating in the presence of a parallelepipedic submerged obstacle. This approach was later used for obliquely incident waves propagating over a submerged trench by Kirby & Dalrymple (1983). More recently, it was extended by Rey (1995) to arbitrary topographies and submerged structures. All these works were based on the linear approximation of the potential equations for free surface flows, in elementary domains of constant depth.

3.1. *Equations of the problem*

It is entirely classical to solve water wave problems using potential theory. In this approach, we seek solutions of the problem fulfilling the Laplace equation

$$\Delta\phi(x, z, t) = 0. \tag{3.1}$$

In the framework of this theory, the fully nonlinear equations corresponding to free surface kinematic and dynamic boundary conditions are given by

$$\frac{\partial \eta}{\partial t} + \frac{\partial \phi}{\partial x}\frac{\partial \eta}{\partial x} = \frac{\partial \phi}{\partial z} \quad \text{on } z = \eta, \tag{3.2}$$

$$\frac{\partial \phi}{\partial t} + \frac{\nabla\phi^2}{2} + g\eta = 0 \quad \text{on } z = \eta. \tag{3.3}$$

These conditions have to be completed with a bottom condition,

$$\frac{\partial \phi}{\partial z} = 0 \quad \text{on } z = -h. \tag{3.4}$$

By using a perturbative approach, we might seek solutions of the form

$$\phi = \varepsilon\phi_1 + \varepsilon^2\phi_2 + O(\varepsilon^3) \tag{3.5}$$

$$\eta = \varepsilon\eta_1 + \varepsilon^2\eta_2 + O(\varepsilon^3), \tag{3.6}$$

where ε is a small parameter corresponding to wave steepness. The equations (3.1)–(3.4) might be simplified to become, to first order in ε,

$$\Delta\phi_1 = 0, \tag{3.7}$$

$$\frac{\partial^2 \phi_1}{\partial t^2} + g\frac{\partial \phi_1}{\partial z} = 0 \quad \text{on } z = 0, \tag{3.8}$$

$$\frac{\partial \phi_1}{\partial z} = 0 \quad \text{on } z = -h. \tag{3.9}$$

From this set of equations, the first-order elevation can be obtained from the first-order velocity potential through the linearized kinematic boundary condition, which reads

$$\frac{\partial \eta_1}{\partial t} = \frac{\partial \phi_1}{\partial z} \quad \text{on } z = 0. \tag{3.10}$$

At the same time, considering terms of second order in ε leads to

$$\Delta\phi_2 = 0, \tag{3.11}$$

$$\frac{\partial^2 \phi_2}{\partial t^2} + g\frac{\partial \phi_2}{\partial z} = -\eta_1 \frac{\partial}{\partial z}\left[\frac{\partial^2 \phi_1}{\partial t^2} + g\frac{\partial \phi_1}{\partial z}\right] - \frac{\partial\,(\nabla\phi_1)^2}{\partial t} \quad \text{on } z = 0, \tag{3.12}$$

$$\frac{\partial \phi_2}{\partial z} = 0 \quad \text{on } z = -h. \tag{3.13}$$

3.2. *Solution of the first-order problem*

The linear problem corresponding to (3.7)–(3.9) might be solved by considering elementary domains of constant depth h_m in which the solutions are known. For problems involving submerged obstacles, two cases must be distinguished. If the upper boundary condition of the domain corresponds to a free surface, (3.8) has to be verified. On the other hand, under the obstacle, a condition of impermeability of the form (3.9) must be fulfilled.

For domains involving a free surface, these solutions are given by the real part of

$$\phi_{1,m}(x, z, t) = \left(\phi^{\pm}_{1p,m}\chi_m(z)\mathrm{e}^{\mathrm{i}k^{\pm}_m x} + \sum_{n=1}^{\infty}\phi^{\pm}_{1e,n,m}\psi_{n,m}(z)\mathrm{e}^{k^{\pm}_{n,m}x}\right)\mathrm{e}^{-\mathrm{i}\omega t}, \tag{3.14}$$

where the subscript m refers to the number of the domain. In this equation, the first term corresponds to propagating modes, in both directions (Ox) and $(-Ox)$, and the second term corresponds to local (or evanescent) modes, $k^{\pm}_m$ and $k^{\pm}_{n,m}$ being the related wavenumbers. Wavenumbers $k^{\pm}_m$ should be understood as k^{+}_m for $k^{\pm}_m > 0$, corresponding to modes propagating in the (Ox) direction, and k^{-}_m for $k^{\pm}_m < 0$, corresponding to modes propagating in the $(-Ox)$ direction. Similarly, $k^{\pm}_{n,m} > 0$ should be understood as $k^{+}_{n,m}$, and correspond to local modes decaying in the $(-Ox)$ direction, while $k^{\pm}_{n,m} < 0$ should be understood as $k^{-}_{n,m}$, and correspond to local modes decaying in the (Ox) direction. These wavenumbers are obtained by solving the dispersion relation

$$\omega^2 = g\kappa\tanh(\kappa h_m), \tag{3.15}$$

with $\kappa = k^{\pm}_m$ for propagating modes, and $\kappa = ik^{\pm}_{n,m}$ for evanescent modes. The functions $\chi_m(z)$ and $\psi_{n,m}(z)$ are given by

$$\chi_m(z) = \frac{\cosh(k^{+}_m(z + h_m))}{\cosh(k^{+}_m h_m)}, \tag{3.16}$$

$$\psi_{n,m}(z) = \frac{\cos(k^{+}_{n,m}(z + h_m))}{\cos(k^{+}_{n,m}h_m)}, \tag{3.17}$$

allowing the solution (3.14) to satisfy the bottom condition for $z=-h_m$. The associated water elevation is thus given by the real part of solution

$$\eta_{1,m}(x,t)=\left(\frac{\mathrm{i}\phi^{\pm}_{1p,m}}{\omega}\chi'_m(z=0)\mathrm{e}^{\mathrm{i}k^{\pm}_m x}+\sum_{n=1}^{\infty}\frac{\mathrm{i}\phi^{\pm}_{1e,n,m}}{\omega}\psi'_{n,m}(z=0)\mathrm{e}^{k^{\pm}_{n,m}x}\right)\mathrm{e}^{-\mathrm{i}\omega t}. \quad (3.18)$$

In the domains involving no free surface, the solutions given by (3.14) are no longer valid, and might be replaced with

$$\phi_{1,m}(x,z,t)=\left(\alpha_m x+\gamma_m+\sum_{n=1}^{\infty}\beta^{\pm}_{n,m}\psi_{n,m}(z)\mathrm{e}^{k^{\pm}_{n,m}x}\right)\mathrm{e}^{-\mathrm{i}\omega t}, \quad (3.19)$$

where $k_{n,m}$ allows satisfaction of the impermeability conditions on both top and bottom conditions. Thus, if h_m still refers to the depth of bottom boundary condition in the mth domain, and if d_m refers to the depth of the upper boundary condition in the mth domain, the wavenumbers $k_{n,m}$ are given by $k^{\pm}_{n,m}=\pm n\pi/(h_m-d_m)$.

These equations (3.14) and (3.19) are solutions of the linear problem defined by (3.7)–(3.9) in each subdomain m. Thus, the solutions should connect continuously at the interface of the domains. To ensure this continuity, conditions of flux $(\partial\phi/\partial x)$ and pressure $(\partial\phi/\partial t=-\mathrm{i}\omega\phi)$ conservation between domains m and $m+1$ are imposed. Specifically, in our case, four domains are defined. Domain 1 extends on $-\infty\leqslant x\leqslant X_6$ and $-h_1\leqslant z\leqslant 0$. Domain 2 corresponds to the fluid domain above the plate, which spreads on $X_6\leqslant x\leqslant X_{12}$ and $-h_2\leqslant z\leqslant 0$. Domain 3 is the fluid domain under the plate, and involves no free surface. This domain ranges from $X_6\leqslant x\leqslant X_{12}$ and $-h_3\leqslant z\leqslant -d_3$. Finally, domain 4 is the domain down-wave of the plate, extending from $X_{12}\leqslant x\leqslant\infty$ and $-h_4\leqslant z\leqslant 0$.

Thus, the boundary conditions between domain 1 and domains 2 and 3 are imposed on $x=X_6$, and read

$$\frac{\partial\phi_{1,1}}{\partial x}=\frac{\partial\phi_{1,2}}{\partial x} \quad \text{and} \quad \phi_{1,1}=\phi_{1,2} \quad \text{for } -h_2\leqslant z\leqslant 0, \quad (3.20)$$

$$\frac{\partial\phi_{1,1}}{\partial x}=0 \quad \text{for } -d_3\leqslant z\leqslant -h_2, \quad (3.21)$$

$$\frac{\partial\phi_{1,1}}{\partial x}=\frac{\partial\phi_{1,3}}{\partial x} \quad \text{and} \quad \phi_{1,1}=\phi_{1,3} \quad \text{for } -h_3\leqslant z\leqslant -d_3. \quad (3.22)$$

Similarly, for $x=X_{12}$, boundary conditions between domains 2 and 3 and domain 4 are given by

$$\frac{\partial\phi_{1,2}}{\partial x}=\frac{\partial\phi_{1,4}}{\partial x} \quad \text{and} \quad \phi_{1,2}=\phi_{1,4} \quad \text{for } -h_2\leqslant z\leqslant 0, \quad (3.23)$$

$$\frac{\partial\phi_{1,4}}{\partial x}=0 \quad \text{for } -d_3\leqslant z\leqslant -h_2, \quad (3.24)$$

$$\frac{\partial\phi_{1,3}}{\partial x}=\frac{\partial\phi_{1,4}}{\partial x} \quad \text{and} \quad \phi_{1,3}=\phi_{1,4} \quad \text{for } -h_3\leqslant z\leqslant -d_3. \quad (3.25)$$

To take advantage of the orthogonality of the eigenfunctions χ_m and $\psi_{n,m}$, these boundary conditions should be written in their integral form, leading to

$$\int_{-h_1}^{0} \frac{\partial \phi_{1,1}}{\partial x}(X_6, z)\, \chi_1(z)\, \mathrm{d}z = \int_{-h_3}^{-d_3} \frac{\partial \phi_{1,3}}{\partial x}(X_6, z)\, \chi_1(z)\, \mathrm{d}z + \int_{-h_2}^{0} \frac{\partial \phi_{1,2}}{\partial x}(X_6, z)\, \chi_1(z)\, \mathrm{d}z, \quad (3.26)$$

$$\int_{-h_1}^{0} \frac{\partial \phi_{1,1}}{\partial x}(X_6, z)\, \psi_{n,1}(z)\, \mathrm{d}z = \int_{-h_3}^{-d_3} \frac{\partial \phi_{1,3}}{\partial x}(X_6, z)\, \psi_{n,1}(z)\, \mathrm{d}z + \int_{-h_2}^{0} \frac{\partial \phi_{1,2}}{\partial x}(X_6, z)\, \psi_{n,1}(z)\, \mathrm{d}z \quad (n = 1, \ldots, \infty) \quad (3.27)$$

for the flux conservation, and

$$\int_{-h_2}^{0} \phi_{1,1}(X_6, z)\, \chi_2(z)\, \mathrm{d}z = \int_{-h_2}^{0} \phi_{1,2}(X_6, z)\, \chi_2(z)\, \mathrm{d}z, \quad (3.28)$$

$$\int_{-h_2}^{0} \phi_{1,1}(X_6, z)\, \psi_{n,2}(z)\, \mathrm{d}z = \int_{-h_2}^{0} \phi_{1,2}(X_6, z)\, \psi_{n,2}(z)\, \mathrm{d}z \quad (n = 1, \ldots, \infty), \quad (3.29)$$

$$\int_{-h_3}^{-d_3} \phi_{1,1}(X_6, z)\, \chi_3(z)\, \mathrm{d}z = \int_{-h_3}^{-d_3} \phi_{1,3}(X_6, z)\, \chi_3(z)\, \mathrm{d}z, \quad (3.30)$$

$$\int_{-h_3}^{-d_3} \phi_{1,1}(X_6, z)\, \psi_{n,3}(z)\, \mathrm{d}z = \int_{-h_3}^{-d_3} \phi_{1,3}(X_6, z)\, \psi_{n,3}(z)\, \mathrm{d}z \quad (n = 1, \ldots, \infty) \quad (3.31)$$

for the pressure conservation. Similarly, on $x = X_{12}$, the boundary conditions are given by their integral form

$$\int_{-h_4}^{0} \frac{\partial \phi_{1,4}}{\partial x}(X_{12}, z)\, \chi_4(z)\, \mathrm{d}z = \int_{-h_3}^{-d_3} \frac{\partial \phi_{1,3}}{\partial x}(X_{12}, z)\, \chi_4(z)\, \mathrm{d}z + \int_{-h_2}^{0} \frac{\partial \phi_{1,2}}{\partial x}(X_{12}, z)\, \chi_4(z)\, \mathrm{d}z, \quad (3.32)$$

$$\int_{-h_4}^{0} \frac{\partial \phi_{1,4}}{\partial x}(X_{12}, z)\, \psi_{n,4}(z)\, \mathrm{d}z = \int_{-h_3}^{-d_3} \frac{\partial \phi_{1,3}}{\partial x}(X_{12}, z)\, \psi_{n,4}(z)\, \mathrm{d}z + \int_{-h_2}^{0} \frac{\partial \phi_{1,2}}{\partial x}(X_{12}, z)\, \psi_{n,4}(z)\, \mathrm{d}z \quad (n = 1, \ldots, \infty) \quad (3.33)$$

for the flux conservation, and

$$\int_{-h_2}^{0} \phi_{1,4}(X_{12}, z)\, \chi_2(z)\, \mathrm{d}z = \int_{-h_2}^{0} \phi_{1,2}(X_{12}, z)\, \chi_2(z)\, \mathrm{d}z, \quad (3.34)$$

$$\int_{-h_2}^{0} \phi_{1,4}(X_{12}, z)\, \psi_{n,2}(z)\, \mathrm{d}z = \int_{-h_2}^{0} \phi_{1,2}(X_{12}, z)\, \psi_{n,2}(z)\, \mathrm{d}z \quad (n = 1, \ldots, \infty), \quad (3.35)$$

$$\int_{-h_3}^{-d_3} \phi_{1,4}(X_{12}, z)\, \chi_3(z)\, \mathrm{d}z = \int_{-h_3}^{-d_3} \phi_{1,3}(X_{12}, z)\, \chi_3(z)\, \mathrm{d}z, \quad (3.36)$$

$$\int_{-h_3}^{-d_3} \phi_{1,4}(X_{12}, z)\, \psi_{n,3}(z)\, \mathrm{d}z = \int_{-h_3}^{-d_3} \phi_{1,3}(X_{12}, z)\, \psi_{n,3}(z)\, \mathrm{d}z \quad (n = 1, \ldots, \infty) \quad (3.37)$$

T	$R_{absorber}$	$L_{absorber}$
1.4	0.01	27.1
1.9	0.15	26.4
2.7	0.12	19.5

TABLE 3. Parameters used to model the influence of the wave absorber.

for the pressure conservation. For numerical implementation, the number of local modes considered is not infinite, but is truncated to a number N. Thus, the system above provides a linear system of $6(N+1)$ equations, allowing us to obtain the $6(N+1)$ unknowns of the problem, which correspond to the complex amplitudes of each mode in each domain. Namely, the unknowns of the problem read $(\phi^-_{1p,1};\ \phi^+_{1e,n,1})$, $(\phi^\pm_{1p,2};\ \phi^\pm_{1e,n,2})$, $(\alpha_3,\ \gamma_3;\ \phi^\pm_{1e,n,3})$, $(\phi^+_{1p,4};\ \phi^-_{1e,n,4})$, $(n=1,\ldots,N)$. In this study, the number of local modes was truncated, e.g. to $N=50$.

Furthermore, as has been discussed in previous work (Rey & Touboul 2011), the influence of the wave absorber can be introduced in the model by considering the presence of a wave propagating in the $(-Ox)$ direction in the last domain. This component amplitude is assumed to be a fraction $R_{absorber}$ of the transmitted component $(\phi^+_{1p,4})$, allowing us to keep the number of unknowns constant. The two propagating modes are assumed to be in phase in a location $L_{absorber}$. These parameters can be understood as reflection at the wave absorber, and its effective location. The parameters used in the present study are detailed in table 3.

Finally, once the linear system is inverted, the amplitude of every mode in every domain is known. The bottom pressure distribution is obtained by evaluating the time derivative of the velocity potential at $z=-h_m$ in every domain

$$\frac{p(x,-h_m,t)}{\rho} = -\frac{\partial \phi_{1,m}}{\partial t}(x,-h_m,t). \tag{3.38}$$

3.3. *Solution of the second-order problem*

By considering the set of equations (3.11)–(3.13), one can see that it admits solutions depending on the first-order solutions. Since the first-order solutions are real, the complex conjugate should not be omitted while deriving the set of equations (3.11)–(3.13). Thus, the solutions of this problem involve oscillatory terms relative to the frequency 2ω $(\mathrm{e}^{2\mathrm{i}\omega t}, \mathrm{e}^{-2\mathrm{i}\omega t})$, and time-independent terms $(\mathrm{e}^{\mathrm{i}\omega t-\mathrm{i}\omega t}=1)$. The latter terms are ignored here, since they are not our concern. The remaining solutions might be understood as interactions of two waves.

Indeed, if considering the interaction of the solution of the first-order problem propagating in the $(0x)$ direction with itself, the solutions are given by the real part of

$$\phi^{++}_{2,m}(x,z,t) = \frac{3\mathrm{i}\omega^3\,(\phi^+_{1p,m})^2}{8\ g^2}\frac{\cosh(2k^+_{1,m}(z+h))}{\sinh^4(k^+_{1,m}h)}\mathrm{e}^{2\mathrm{i}k^+_{1,m}x}\mathrm{e}^{-2\mathrm{i}\omega t}, \tag{3.39}$$

where $k^+_{1,m}$ is the solution of (3.15) corresponding to waves propagating in the (Ox) direction in the mth domain. This term is the well-known second-order Stokes' wave solution. Symmetrically, we identify the solution corresponding to the interaction of waves propagating in the $(-Ox)$ direction, and it becomes

$$\phi_{2,m}^{--}(x, z, t) = \frac{3\mathrm{i}\omega^3 \left(\phi_{1p,m}^{-}\right)^2}{8g^2} \frac{\cosh(2k_{1,m}^{-}(z+h))}{\sinh^4(k_{1,m}^{-}h)} \mathrm{e}^{2\mathrm{i}k_{1,m}^{-}x} \mathrm{e}^{-2\mathrm{i}\omega t}. \tag{3.40}$$

Here again, the solution is given by considering the real part of expression (3.40). The interaction of waves propagating in the (Ox) direction and the $(-Ox)$ direction leads to the second-order term

$$\phi_{2,m}^{+-}(x, z, t) = -\frac{\mathrm{i}\omega^3 (\phi_{1p,m}^{+} \times \phi_{1p,m}^{-})}{4g^2} \frac{2\cosh(2k_{1,m}^{+}h) - 1}{\sinh^2(k_{1,m}^{+}h)} \mathrm{e}^{-2\mathrm{i}\omega t}. \tag{3.41}$$

This term, originally introduced by Longuet-Higgins (1950), is surprising since it does not depend on z. It will lead to a pressure disturbance oscillating at a frequency 2ω, and propagating independently of the depth.

Following Longuet-Higgins' approach, we might take into account the interaction of propagative modes together with local modes. This leads to the derivation of a term given by

$$\begin{aligned}\phi_{2,m}^{e+}(x, z, t) &= \frac{\omega^3 (\phi_{1p,m}^{+} \times \phi_{1e,n,m}^{\pm})}{g^2} \\ &\times \frac{\sinh^2(k_{1,m}^{+}h) - \sin^2(k_{1,n,m}^{\pm}h) - 4\mathrm{i}\sinh(k_{1,m}^{+}h)\sin(k_{1,n,m}^{\pm}h)\cosh((k_{1,m}^{+} + \mathrm{i}k_{1,n,m}^{\pm})h)}{\sinh^2(k_{1,m}^{+} - \mathrm{i}k_{1,n,m}^{\pm})h) + 4\mathrm{i}\sinh(k_{1,m}^{+}h)\sin(k_{1,n,m}^{\pm}h)\cosh((k_{1,m}^{+} - \mathrm{i}k_{1,n,m}^{\pm})h)} \\ &\times \frac{\cosh((k_{1,m}^{+} - \mathrm{i}k_{1,n,m}^{\pm})(z+h))}{\sinh(k_{1,m}^{+}h)\sin(k_{1,n,m}^{\pm}h)} \mathrm{e}^{(\mathrm{i}k_{1,m}^{+} + k_{1,n,m}^{\pm})x - 2\mathrm{i}\omega t},\end{aligned} \tag{3.42}$$

for the interaction of waves propagating in the (Ox) direction with local modes, or

$$\begin{aligned}\phi_{2,m}^{e-}(x, z, t) &= \frac{\omega^3 (\phi_{1p,m}^{-} \times \phi_{1e,n,m}^{\pm})}{g^2} \\ &\times \frac{\sinh^2(k_{1,m}^{-}h) - \sin^2(k_{1,n,m}^{\pm}h) - 4\mathrm{i}\sinh(k_{1,m}^{-}h)\sin(k_{1,n,m}^{\pm}h)\cosh((k_{1,m}^{-} + \mathrm{i}k_{1,n,m}^{\pm})h)}{\sinh^2(k_{1,m}^{-} - \mathrm{i}k_{1,n,m}^{\pm})h) + 4\mathrm{i}\sinh(k_{1,m}^{-}h)\sin(k_{1,n,m}^{\pm}h)\cosh((k_{1,m}^{-} - \mathrm{i}k_{1,n,m}^{\pm})h)} \\ &\times \frac{\cosh((k_{1,m}^{-} - \mathrm{i}k_{1,n,m}^{\pm})(z+h))}{\sinh(k_{1,m}^{-}h)\sin(k_{1,n,m}^{\pm}h)} \mathrm{e}^{(\mathrm{i}k_{1,m}^{-} + k_{1,n,m}^{\pm})x - 2\mathrm{i}\omega t},\end{aligned} \tag{3.43}$$

for the interaction of waves propagating in the $(-Ox)$ direction with local modes. Here again, one should keep in mind that the real part of this expression has to be considered.

Finally, by taking account of local modes interacting together, we obtain a solution of the form

$$\begin{aligned}\phi_{2,m}^{ee}(x, z, t) &= \frac{\mathrm{i}\omega^3 (\phi_{1e,n,m}^{\pm} \times \phi_{1e,l,m}^{\pm})}{4g^2} \\ &\times \frac{\sin^2(k_{1,n,m}^{\pm}h) + \sin^2(k_{1,l,m}^{\pm}h) + 4\sin(k_{1,n,m}^{\pm}h)\sin(k_{1,l,m}^{\pm}h)\cos((k_{1,n,m}^{\pm} - k_{1,l,m}^{\pm})h)}{\sin^2((k_{1,n,m}^{\pm} + k_{1,l,m}^{\pm})h) - 4\sin(k_{1,n,m}^{\pm}h)\sin(k_{1,l,m}^{\pm}h)\cos((k_{1,n,m}^{\pm} + k_{1,l,m}^{\pm})h)} \\ &\times \frac{\cos((k_{1,n,m}^{\pm} + k_{1,l,m}^{\pm})(z+h))}{\sin(k_{1,n,m}^{\pm}h)\sin(k_{1,l,m}^{\pm}h)} \mathrm{e}^{(k_{1,n,m} + k_{1,l,m})x} \mathrm{e}^{-2\mathrm{i}\omega t}.\end{aligned} \tag{3.44}$$

Thus, the velocity potential

$$\phi_{2,m,forced}(x,z,t) = \phi_{2,m}^{++} + \phi_{2,m}^{--} + \phi_{2,m}^{+-} + \sum_{n=1}^{N} \left(\phi_{2,m}^{e+} + \phi_{2,m}^{e-}\right) + \sum_{n=1}^{N}\sum_{l=1}^{N} \phi_{2,m}^{ee} \tag{3.45}$$

is the solution of the set of equations (3.11)–(3.13), and is known as soon as the first-order problem is solved.

It has to be mentioned that the double summation in (3.45) is found to be diverging as $N \to \infty$, which is consistent with the asymptotic behaviour of $k_{1,n,m}^{\pm}$, when $n \to \infty$. As a result, these local mode couplings correspond to a singularity which should be properly extracted. This result is not really surprising, since these modes are not solutions to the problem on the interfaces of the domains. However, the weight of the local modes in the solution is known to be rapidly decreasing. Thus, we assumed the same behaviour for their nonlinear interaction, and we decided to neglect this term in the following.

Once the solution imposed by first order is known, one has to keep in mind that each elementary domain m still admits linear solutions of (3.7)–(3.9), relative to the frequency 2ω,

$$\phi_{2,m}(x,z,t) = \left(\phi_{2p,m}^{\pm}\chi_m(z)\mathrm{e}^{\mathrm{i}k_m^{\pm}x} + \sum_{n=1}^{\infty} \phi_{2e,n,m}^{\pm}\psi_{n,m}(z)\mathrm{e}^{k_{n,m}^{\pm}x}\right)\mathrm{e}^{-2\mathrm{i}\omega t}, \tag{3.46}$$

where $k_m^{\pm}$ and $k_{n,m}^{\pm}$ are now obtained by solving the linear dispersion relation

$$4\omega^2 = g\kappa\tanh(\kappa h_m). \tag{3.47}$$

A linear system very similar to that obtained for the first-order problem can be obtained by imposing the continuity conditions of velocity and pressure. However, the velocity potential (3.45) obtained by considering the nonlinear interaction of first-order terms is involved in these new boundary conditions. The solution of this linear system provides the amplitude of each second-order mode, and the associated bottom pressure is given by

$$\frac{p(x,-h_m,t)}{\rho} = -\left(\frac{\partial\phi_{2,m}}{\partial t} + \frac{\partial\phi_{2,m,forced}}{\partial t} + \frac{\nabla\phi_{1,m}^2}{2}\right)(x,-h_m,t). \tag{3.48}$$

In the following, computations are obtained with a truncation of evanescent modes, e.g. to $N = 50$.

4. Results and discussion

Results obtained experimentally and analytically are presented in figures 2–4. These three figures represent various depth conditions for incident water waves. Waves of period $T_1 = 1.4$ s have a depth parameter $kh = 6.18$, those of period $T_2 = 1.9$ s have a depth parameter $kh = 3.36$, while waves of period $T_3 = 2.7$ correspond to $kh = 1.77$. In these figures, the dynamic pressure excess is normalized by

$$P_N = \frac{\rho g a_i}{\cosh(kh)}, \tag{4.1}$$

which corresponds to the dynamic pressure amplitude on the bottom associated with the incident wave at frequency f.

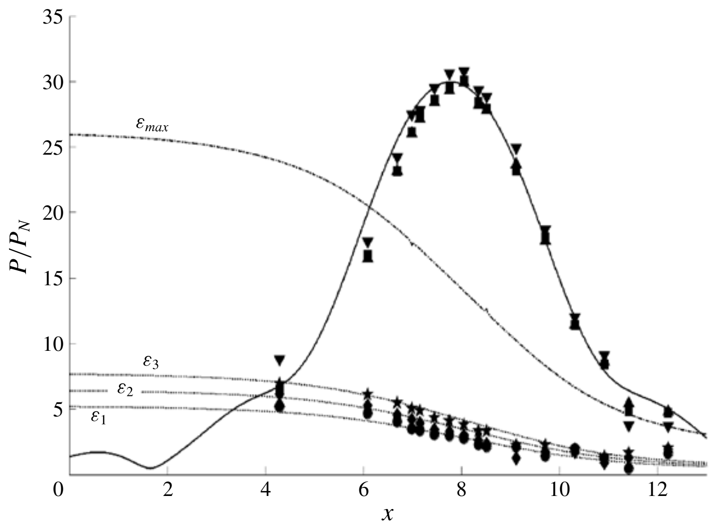

FIGURE 2. Pressure distribution on $z = -h$ obtained experimentally (symbols) and analytically (lines) for incident water waves of period $T_1 = 1.4$ s. The related steepness is given by $\varepsilon_1 = 0.09$, $\varepsilon_2 = 0.11$, and $\varepsilon_3 = 0.13$. ▼, ■, and ▲ represent first-order pressure disturbances obtained experimentally with waves of steepness ε_1, ε_2 and ε_3 respectively. The solid line represents the associated first-order theory. ●, ♦, and ⋆ represent second-order pressure disturbances obtained experimentally with waves of steepness ε_1, ε_2 and ε_3 respectively. The dotted lines represent the associated second-order theory. The dash-dotted line represents the second-order theory that might be obtained with incident waves of limit steepness $\varepsilon_{max} = 0.44$.

Experimental pressure oscillations at the fundamental frequency, which are described by the first-order theory, are plotted as symbols (▼, ■, ▲). The associated first-order model is shown by solid lines. The figures clearly show very good agreement between theory and experiments. We observe that the dynamic pressure excess due to the presence of the obstacle is significant in the deep water case, and decreases with the depth parameter. Pressure oscillations observed for waves propagating in the deep water case are up to thirty times larger than in the absence of submerged structure. For the intermediate depth parameter, the dynamic pressure excess is up to 3.5, and the disturbance associated with the smallest depth parameter is rather a low pressure ($P/P_N = 0.2$). The choice of the normalization made here is interesting, since it emphasizes the role of the structure as compared to the wave-induced bottom pressure in its absence. However, it is interesting to notice that this effect is significant, as compared to the free surface deformation. These bottom pressure variations are significant in each case since they correspond respectively to 13, 25 and 7 % of $\rho g a_i$, for $kh = 6.18$, $kh = 3.36$ and $kh = 1.76$.

This extremum of pressure excess is observed in the vicinity of the plate location ($6.985 < X < 8.515$). This phenomenon is due to the influence of both the evanescent modes and the horizontally oscillating water column under the structure. It is interesting to note the wide extent of this pressure excess deviation, relative to the extent of the plate (1.53 m). This must be compared with the evanescent wavenumber. Further away from the plate, the pressure envelope is found to be oscillating in space. This is due to the presence of the partially standing wave. The associated reflection

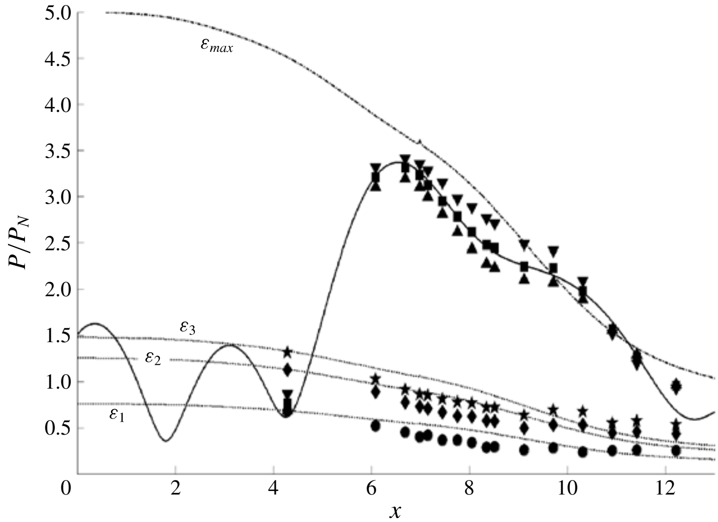

FIGURE 3. Pressure distribution on $z = -h$ obtained experimentally (symbols) and analytically (lines) for incident water waves of period $T_2 = 1.9$ s. The related steepness is given by $\varepsilon_1 = 0.07$, $\varepsilon_2 = 0.11$, and $\varepsilon_3 = 0.13$. ▼, ■, and ▲ represent first-order pressure disturbances obtained experimentally with waves of steepness ε_1, ε_2 and ε_3 respectively. The solid line represents the associated first-order theory. ●, ♦, and ⋆ represent second-order pressure disturbances obtained experimentally with waves of steepness ε_1, ε_2 and ε_3 respectively. The dotted lines represent the associated second-order theory. The dash-dotted line represents the second-order theory that might be obtained with incident waves of limit steepness $\varepsilon_{max} = 0.44$.

coefficients are found to be $R = 0.13$ for $kh = 6.18$, $R = 0.46$ for $kh = 3.36$ and $R = 0.24$ for $kh = 1.76$, respectively. For wave periods $T_2 = 1.9$ s and $T_3 = 2.7$, the reflection coefficients of the wave absorber are significant, and slightly dependent on the wave steepness. Indeed, a slight vertical shift is observed in both figures 3 and 4, since we decided to keep these parameters constant for the calculation at each given frequency (see table 3).

Pressure oscillations at the second harmonic frequency $2f$ are described by the second-order theory. In figures 2, 3 and 4, the experimental results are plotted with symbols (●, ♦, ⋆), while the second-order theory is shown by dotted lines. In addition to these lines, a dashed line is plotted to represent the limit case, associated with an incident wave of steepness $\varepsilon = 0.44$. In every case, the theoretical results are in good agreement with the experimental data. Here again, we observe that the second-order pressure disturbance due to the presence of the obstacle is significant in the deep water case, and decreases with the depth parameter. Since this nonlinear effect is proportional to the wave steepness, relative pressure variations might reach values up to 26 for the deep water case, 5 for the intermediate water case, and 0.2 for the shallowest water conditions.

In every case, the maximum value is observed up-wave, far from the plate. This fact tends to emphasize the relative importance of the propagative–propagative mode interaction (e.g. the Longuet-Higgins term). Down-wave, between the plate and the wave absorber, the asymptotic value is lower than up-wave. This is explained by the low value of the absorber reflection. For the shallowest case, a relatively important

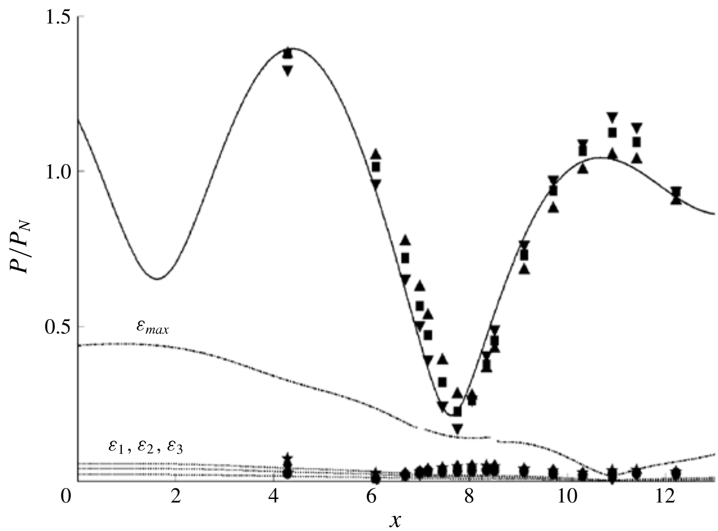

FIGURE 4. Pressure distribution on $z = -h$ obtained experimentally (symbols) and analytically (lines) for incident water waves of period $T_2 = 2.7$ s. The related steepness is given by $\varepsilon_1 = 0.02$, $\varepsilon_2 = 0.04$ and $\varepsilon_3 = 0.06$. ▼, ■, and ▲ represent first-order pressure disturbances obtained experimentally with waves of steepness ε_1, ε_2 and ε_3 respectively. The solid line represents the associated first-order theory. ●, ♦, and ⋆ represent second-order pressure disturbances obtained experimentally with waves of steepness ε_1, ε_2 and ε_3 respectively. The dotted lines represent the associated second-order theory. The dash–dotted line represents the second-order theory that might be obtained with incident waves of limit steepness $\varepsilon_{max} = 0.44$.

value is also observed under the plate, which tends to emphasize the role of the propagative–evanescent mode interaction in the nonlinear forcing.

5. Concluding remarks

In this work, the distribution of the dynamic pressure excess due to wave scattering on a submerged horizontal plate was investigated for various wave steepnesses ε and water depth conditions kh. This case study was of particular theoretical interest, since it involved partially standing wave conditions, evanescent modes, and a horizontally oscillating water column.

The first-order bottom distribution of the pressure excess, corresponding to the fundamental frequency f of the incident wave, was found to be significant even for incoming waves in deep water conditions. In the case of waves presenting a depth parameter $kh = 6.16$, the bottom dynamic pressure excess was, surprisingly, found to be thirty times larger than expected in the absence of the plate. This behaviour is explained via the role of evanescent modes and a horizontally oscillating water column under the plate. Indeed, these local modes still exist whatever the water depth, as shown by (3.14) and (3.19). Thus, similar phenomena at first order might be observed under floating bodies (free or fixed), near steep slopes, or for any other configuration leading to the generation of these local modes.

The bottom pressure distribution oscillating at the frequency $2f$, and corresponding to second order in nonlinearity, was also found to be important. In some cases, it was found to be of the same order as first-order distribution. It was interpreted as the forcing due to the nonlinear interaction between the wave components. The relative value of the second-order dynamic pressure excess distribution decreases with decreasing kh. This behaviour cannot be fully ascribed to the rate of the standing wave, since important reflection coefficients are observed for waves in relative water depth conditions $kh = 1.76$.

However, variations of the wave-induced bottom pressure distribution were found to be significant depending on wave conditions. In addition, such gradients in dynamic pressure distributions may have a significant impact on the dynamics of sandy beds, or wave energy tapping devices. Further studies on locally induced sediment transport due to near-bed oscillations of the fluid are in progress.

Acknowledgements

The authors are grateful to the Conseil Général du Var for its financial support for the experiments carried out in the BGO FIRST wave basin in the framework of the GIS HYDRO.

REFERENCES

ARDHUIN, F., STUTZMANN, E., SCHIMMEL, M. & MANGENEY, A. 2011 Ocean wave sources of seismic noise. *J Geophys. Res.* **116**, C09004.

ATHANASSOULIS, G. A. & BELIBASSAKIS, K. A. 1999 A consistent coupled-mode theory for the propagation of small-amplitude water waves over variable bathymetry regions. *J. Fluid Mech.* **389**, 275–301.

BELIBASSAKIS, K. A. & ATHANASSOULIS, G. A. 2006 A coupled-mode technique for weakly nonlinear wave interaction with large floating structures lying over variable bathymetry regions. *Appl. Ocean Res.* **28** (1), 59–76.

BISHOP, C. T. & DONELAN, M. A. 1987 Measuring waves with pressure transducers. *Coast. Engng* **11**, 309–328.

CAVALERI, L. 1980 Wave measurements using pressure transducer. *Oceanol. Acta* **3** (3), 339–346.

ESCHER, J. & SCHLURMANN, T. 2008 On the recovery of the free surface from the pressure within periodic travelling water waves. *J. Nonlinear Math. Phys.* **15** (2), 50–57.

FARRELL, W. E. & MUNK, W. 2008 What do deep sea pressure fluctuations tell about short surface waves? *Geophys. Res. Lett.* **35**, L19605.

FARRELL, W. E. & MUNK, W. 2010 Booms and busts in the deep. *J. Phys. Oceanogr.* **40**, 2159–2169.

GODA, Y. & SUZUKI, Y. 1976 Estimation of incident and reflected waves in random wave experiments. In *Proceedings of the 15th Coastal Engineering Conference*, pp. 828–845. Coastal Engineering Research Council.

GRACE, R. A. 1978 Surface wave heights from pressure records. *Coast. Engng* **2**, 55–67.

GRUE, J. & PALM, E. 1984 Reflection of surface waves by submerged cylinders. *Appl. Ocean Res.* **6** (1), 54–60.

GUAZZELLI, E., REY, V. & BELZONS, M. 1992 Higher order Bragg reflection of surface gravity waves by periodic beds. *J. Fluid Mech.* **245**, 301–317.

GUEVEL, P., LANDEL, E., BOUCHET, R. & MANZONE, J. M. 1986 Techniques nouvelles de brise houle et de protection des sites côtiers. Part I. Le phénomène d'un mur d'eau oscillant et son application pour protéger un site côtier soumis à l'action de la houle. *Bull. Permanent International Association of Navigation Congresses***52**, 48–59..

HASSELMANN, K. 1963 A statistical analysis of the generation of microseisms. *Rev. Geophys.* **1**, 177–210.

KEDAR, S., LONGUET-HIGGINS, M. S., GRAHAM, F. W. N., CLAYTON, R. & JONES, C. 2008 The origin of deep ocean microseisms in the North Atlantic Ocean. *Proc. R. Soc. Lond. Ser.* A **464**, 1–35.

KIRBY, J. T. & DALRYMPLE, R. D. 1983 Propagation of obliquely incident water waves over a trench. *J. Fluid Mech.* **133**, 419–443.

LAN, Y. J., HSU, T. W., LAI, J. W., CHANG, C. C. & TING, C. H. 2011 Bragg scattering of waves propagating over a series of poro-elastic submerged breakwaters. *Wave Mot.* **48**, 1–12.

LEE, J. F. & LAN, Y. J. 2002 On waves propagating over poro-elastic seabed. *Ocean Engng* **29** (8), 931–946.

LONGUET-HIGGINS, M. S. 1950 A theory of the origin of microseisms. *Proc. R. Soc. Lond. Ser* A **243**, 1–35.

MAGNE, R., BELIBASSAKIS, K. A., HERBERS, T. H. C., ARDHUIN, F., O'REILLY, W. C. & REY, V. 2007 Evolution of surface gravity waves over a submarine canyon. *J. Geophys. Res.* **112**, C01002.

MANSARD, E. P. D. & FUNKE, E. R. 1980 The measurement of incident and reflected spectra using a least square method. In *Proceedings of the 15th Coastal Engineering Conference*, pp. 154–172.

MICHE, M. 1944 Mouvements ondulatoires de la mer en profondeur croissante ou décroissante. *Ann. Ponts Chauss.* **2**, 131–164.

MOLIN, B., LAJOIE, D., JARRY, N. & ROUSSEAUX, G. 2008 Tapping wave energy through Longuet-Higgins microseism effect. In *Proceedings of the 23rd International Workshop on Water Waves and Floating Bodies*, pp. 132–135.

NEWMAN, J. N. 1990 Second-harmonic wave diffraction at large depths. *J. Fluid Mech.* **213**, 59–70.

NIELSEN, P. 1989 Analysis of natural waves by local approximation. *J. Waterway Port Coast. Engng* **115** (3), 384–397.

REY, V. 1992 Propagation and local behaviour of normally incident gravity waves over varying topography. *Eur. J. Mech.* B **11** (2), 213–232.

REY, V. 1995 A note on the scattering of obliquely incident gravity waves by cylindrical obstacles in waters of finite depth. *Eur. J. Mech.* B **14** (1), 207–216.

REY, V., CAPIOBIANCO, R. & DULOU, C. 2002 Wave scattering by a submerged plate in presence of a steady uniform current. *Coast. Engng* **47**, 27–34.

REY, V. & TOUBOUL, J. 2011 Forces and moment on a horizontal plate due to regular and irregular waves in the presence of current. *Appl. Ocean Res.* **33** (2), 88–99.

SILVESTER, R. & HSU, J. R. C. 1989 Sines revisited. *J. Waterway Port Coast. Engng* **115**, 327–343.

SUMER, B. M., WHITEHOUSE, R. J. S. & TORUM, A. 2001 Scour around coastal structures: a summary of recent research. *Coast. Engng* **44**, 153–190.

TAKANO, K. 1960 Effet d'un obstacle parallélépipédique sur la propagation de la houle. *Houille Blanche* **15**, 247–267.

TSAI, C. P. 1995 Wave induced liquefaction potential in front of a breakwater. *Ocean Engng* **22** (1), 1–18.

TSAI, C. P., HUANG, M. C., YOUNG, F. J., LIN, Y. C. & LI, H. W. 2005 On the recovery of surface wave by pressure transfer function. *Ocean Engng* **32**, 1247–1259.

WANG, H., LEE, D. Y. & GARCIA, A. 1986 Time series surface-wave records from pressure gauge. *Coast. Engng* **10**, 379–393.

WIECHERT, E. 1904 Discussion, Verhandlung der zweiten Internationalen Seismologischen Konferenz. *Beiträge Geophys.* **2**, 41–43.

YAMAMOTO, T., KONING, H. L., SELLMEIJER, H. & HIJUM, E. VAN 1978 On the response of a poro-elastic bed to water waves. *J. Fluid Mech.* **87**, 193–206.